Tunable electronic and magneto-optical properties of monolayer arsenene: From GW_0 approximation to large-scale tight-binding propagation simulations

Jin Yu,[1,2,*] Mikhail I. Katsnelson,[2] and Shengjun Yuan[3,1,2,*]
[1]*Beijing Computational Science Research Center, Beijing 100094, China*
[2]*Theory of Condensed Matter, Radboud University, Nijmegen 6525AJ, The Netherlands*
[3]*School of Physics and Technology, Wuhan University, Wuhan 430072, China*

(Received 5 June 2018; revised manuscript received 15 July 2018; published 11 September 2018)

Monolayers of the group called VA elements have attracted great attention with the rising of black phosphorus. Here, we derive a simple tight-binding model for monolayer grey arsenic, referred to as arsenene (ML-As), based on the first-principles calculations within the partially self-consistent GW_0 approach. The resulting band structure derived from the six p-like orbitals coincides with the quasiparticle energy from GW_0 calculations with a high accuracy. In the presence of a perpendicular magnetic field, ML-As exhibits two sets of Landau levels linear with respect to the magnetic field and level index. Our numerical calculation of the optical conductivity reveals that the obtained optical gap is very close to the GW_0 value and can be effectively tuned by external magnetic field. Thus, our proposed TB model can be used for further large-scale simulations of the electronic, optical, and transport properties of ML-As.

DOI: 10.1103/PhysRevB.98.115117

I. INTRODUCTION

In the past few years, two-dimensional (2D) materials have attracted great attention, from graphene to transition metal dichalcogenides, black phosphorus, layered boron, mixed metal carbides, etc. [1–5] As a precursor of monolayers composed of a group of VA elements, black phosphorus is reported to have potential applications in optoelectronics devices and field effect transistors, owing to its appropriate band gap and excellent electronic properties including a high carrier mobility and on-off current ratio [3]. First-principles calculations on this group of VA element monolayers have shown that their energy gap covers a wide range from 0.36 to 2.62 eV with the carrier mobility varying from $\sim$10 to $\sim 10^4\ \mathrm{cm^2\ V^{-1}\ s^{-1}}$ [6–9]. One of the group of VA elements is arsenic, the binary compound of which, gallium arsenide (GaAs), has been widely known in the semiconducting industry in the last century [10,11]. Meanwhile, monolayer arsenic, namely arsenene, has been receiving continuous interest very recently [12–16]. When it is exploited from bulk gray arsenic into few layers, even into monolayer arsenene (ML-As), it undergoes a transition from metal to semiconductor [17]. The indirect energy gap can be tuned into direct energy gap under biaxial strain [12,17,18]. When the strain is large enough (around 11.7%), theoretically, monolayer arsenene will become a nontrivial topological insulator with a sizable bulk gap up to several tenths of 1 eV [19], which is much higher than traditional 2D materials like graphene [20], silicone, and germanene by one or two orders of magnitude [21,22]. An external electric field, which is used as an effective way to tune the electronic properties, is found to introduce topological phase transition in ML-As [23]. It is also reported that by passivation of halogen atoms and functional groups like CH_3 and OH, one can introduce the quantum spin-Hall effect in arsenene [24–26]. Moreover, strain-tunable magnetism is predicted in ML-As with either electron or hole doping [27].

The physical properties of ML-As have been studied extensively by density functional theory (DFT) investigations [28,29], which is applicable only for the systems with not too high number of nonequivalent atomic positions (up to 10^3). On the contrary, the electronic, optical, transport, and plasmonic properties of various 2D materials can be studied efficiently within the framework of the tight-binding approximation without any symmetry restrictions up to 10^9 atoms [30]. There have been successfully fitted tight-binding models for the group of VA elements P and Sb [31,32], however, an effective tight-binding model for ML-As is still missing. Considering the fact that the binding energy of the first bound exciton of ML-As is evaluated on the order of 0.7 eV when the electron-hole interaction is taken into account [33], the many-body effect is crucially important in altering the optical properties of this 2D material, so it is essential to build a tight-binding model (TB) for ML-As based on the quasiparticle energy beyond density functional.

In this paper, we present a suitable model Hamiltonian governing the low-energy band structure of ML-As and show that its electronic and magneto-optical properties can be tuned by a perpendicular magnetic field. Our first-principles calculations show that the low-energy electronic properties of ML-As is mainly contributed by the $3p$ orbitals of the As atom. Therefore, a set of hybrid p-like orbitals generated by maximally localized Wannier functions (WFs) [34,35] are chosen as the basis to construct the simple TB model for ML-As. The resulting band structure and electron density of states are in good agreement with the one obtained from the interpolation of the results obtained from the GW_0 calculations.

*Author to whom correspondence should be addressed: j.yu@science.ru.nl; s.yuan@whu.edu.cn

We further use the fitted TB model to study the electronic and optical properties of large-scale ML-As under the external magnetic field, in which the ML-As exhibits highly degenerate equidistant Landau levels and tunable magneto-optical conductivities.

II. COMPUTATIONAL METHOD

To construct a reliable TB model for ML-As, we performed first-principles calculations to calibrate the effective Hamiltonian, which is carried out by the Vienna *ab initio* simulation package (VASP) code [36,37]. The vacuum distance between two adjacent ML-As was set to be at least 1.5 nm to avoid interlayer interaction. The generalized gradient approximation [38] was used in combination with the projected augmented-wave method [39]. The plane-wave cutoff energy was set to 260.9 eV. A $25 \times 25 \times 1$ Monkhorst-Pack grid was used for the Brillouin zone sampling for both the relaxation and static calculations. All the atoms were fully relaxed until the force on each atom was less than 0.01 eV/Å. WANNIER90 code [40] was used to construct the Wannier functions and TB parametrization of the DFT Hamiltonian. The obtained hopping parameters are further discarded and reoptimized through a least-squares fitting of the band structure. The electronic density of states (Landau level spectrum) and the magneto-optical conductivity under external magnetic field was calculated using the tight-binding propagation method (TBPM), which is based on the numerical solution of the time-dependent Schrödinger equation without the diagonalization of the Hamiltonian matrix, and very efficient in the calculations of the electronic, transport, and optical properties of large quantum systems with more than millions of atoms [30,41,42].

III. RESULTS AND DISCUSSION

The optimized atomic structure of ML-As is shown in Fig. 1, which has a hexagonal unit cell with the space group being $R\bar{3}m$. The basic unit block contains two sublattices occupied by one As atom per site. After structure optimization, the lattice constant of ML-As is calculated to be $\boldsymbol{a} = \boldsymbol{b} = 3.61$ Å with the out-of-plane buckling of two sites being $\Delta = 1.40$ Å, which is in agreement with previous DFT calculations [33]. Standard DFT calculation shows that ML-As is a semiconductor with an indirect energy gap around 1.60 eV,

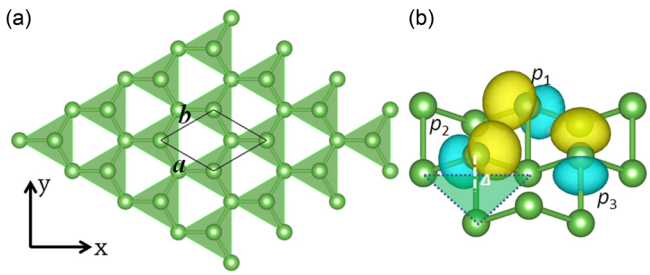

FIG. 1. Atomic structure of ML-As. (a) Top view of ML-As with the unit cell indicated by the black rhombus. The green balls are arsenic atoms. (b) Real-space distribution of the WFs at one sublattice, where three p-like orbitals are situated.

and the valence band maximum (VBM) situates right at the high symmetric Γ point while the conduction band minimum (CBM) situates between Γ and M. The orbital decomposed band structure from DFT calculations shows that the first three valence (VBs) and conduction bands (CBs) are mainly composed of the $3p$ orbitals of As and that they are separated from the other states, which makes it possible for us to build an accurate description of an effective Hamiltonian for ML-As. Thus, we will focus on the six bands in the low-energy regime. To get a more accurate description of the quasiparticle energy, we further performed GW_0 calculations on the electronic structure. A much larger energy gap is calculated to be 2.75 eV. Our parametrization procedure in this work is based on the formalism of maximally localized Wannier functions (MLWFs) [34,35] and six hybrid p-like orbitals are obtained as the basis for the TB model. In Fig. 1(b), we visualize the real-space distribution of the WFs at one site, where a combination of three equivalent p-like orbitals are situated around at the same site of As with a rotation symmetry of $2\pi/3$.

Our nonrelativistic TB model is given by an effective Hamiltonian of

$$H_0 = \sum_{mn} \sum_{ij} t_{ij}^{mn} a_{im}^{\dagger} a_{jn}, \tag{1}$$

where t_{ij}^{mn} is the effective hopping parameter describing the interaction between m and n orbitals residing at atoms i and j, respectively, and $a_{im}^{\dagger}$ (a_{jn}) is the creation (annihilation) operator of an electron at atom i (j) and orbital m (n). To make the TB model simple but accurate enough, we discard the hoppings with an interatomic distance larger than 5.69 Å and the hoppings with amplitudes $|t_i| < 0.07$ eV are ignored as well. The residual hopping parameters are further reoptimized by minimizing the following least-squares function:

$$\delta(\{t_i\}) = \sum_{n,\boldsymbol{k}} \left[E_{n,\boldsymbol{k}}^{GW_0}(\{t_i\})^2 - E_{n,\boldsymbol{k}}^{TB}(\{t_i\})^2 \right] \Big/ \left| E_{n,\boldsymbol{k}}^{GW_0}(\{t_i\}) \right|, \tag{2}$$

where $\{t_i\}$ are the hoppings in Eq. (1) and $E_{n,\boldsymbol{k}}^{GW_0}(\{t_i\})$ ($E_{n,\boldsymbol{k}}^{TB}(\{t_i\})$) corresponds to the eigenvalues of the GW_0 (TB) Hamiltonian with n and $\boldsymbol{k}$ being the band index and momenta along the high-symmetry K points in the first Brillouin zone, respectively. The final hoppings $\{t_i\}$ used in our calculations are schematically shown in Fig. 2 and Table I.

In Eq. (1), we define the Hamiltonian with a 6×6 matrix for ML-As, which can be explicitly solved to get the eigenvalues and eigenvectors. Considering the inversion symmetry, the Hamiltonian matrix can be simply written as

$$H(\boldsymbol{k}) = \begin{pmatrix} U(\boldsymbol{k}) & T(\boldsymbol{k}) \\ T^{\dagger}(\boldsymbol{k}) & U(\boldsymbol{k}_r) \end{pmatrix}, \tag{3}$$

where $U(\boldsymbol{k})$ and $T(\boldsymbol{k})$ are 3×3 matrices describing the intra- and intersublattice hoppings, respectively, and the subscript r in $U(\boldsymbol{k}_r)$ indicates the inversion operation in $U(\boldsymbol{k})$. As the three basic orbitals are rotationally symmetric like a regular triangle, the corresponding matrices in Eq. (3) are

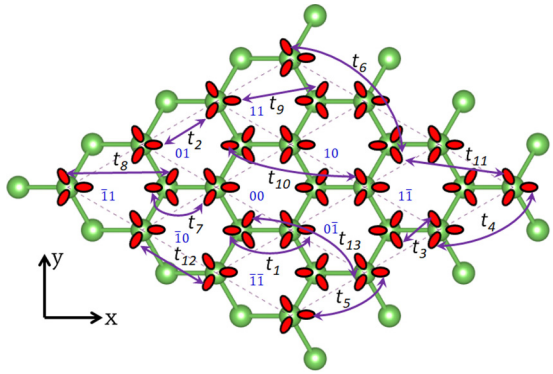

FIG. 2. Hopping diagram in the TB model of ML-As. The orbitals are represented by the negative part of the p-like orbitals as indicated by the red ellipses.

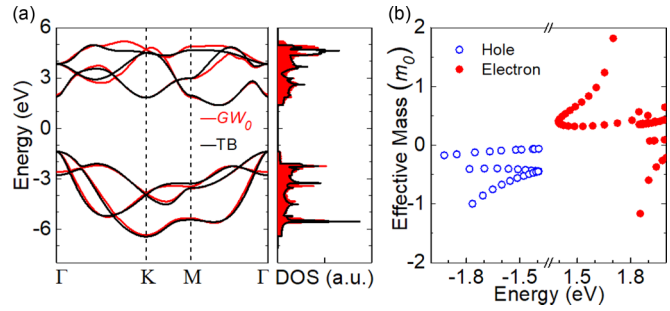

FIG. 3. Electronic properties of ML-As. (a) Band structure and DOS of ML-As. The red and black colors present the GW_0 and TB results, respectively. (b) Effective mass of carriers derived from the TB model in the unit of free electron mass m_0. The EMs of the first CB (electron) and first two VBs (hole) are presented in red and blue, respectively.

expanded as

$$U(\boldsymbol{k}) = \begin{pmatrix} A(\boldsymbol{k}) & B(\boldsymbol{k}) & B^*(\bar{\bar{\boldsymbol{k}}}) \\ B^*(\boldsymbol{k}) & A(\bar{\boldsymbol{k}}) & B(\bar{\boldsymbol{k}}) \\ \bar{\bar{B}}(\boldsymbol{k}) & B^*(\bar{\boldsymbol{k}}) & \bar{\bar{A}}(\boldsymbol{k}) \end{pmatrix}, \tag{4}$$

and

$$T(\boldsymbol{k}) = \begin{pmatrix} C(\boldsymbol{k}) & D(\boldsymbol{k}) & D(\bar{\bar{\boldsymbol{k}}}) \\ D(\boldsymbol{k}) & C(\bar{\boldsymbol{k}}) & D(\bar{\boldsymbol{k}}) \\ \bar{\bar{D}}(\boldsymbol{k}) & D(\bar{\boldsymbol{k}}) & \bar{\bar{C}}(\boldsymbol{k}) \end{pmatrix}, \tag{5}$$

where $\bar{\boldsymbol{k}}$ and $\bar{\bar{\boldsymbol{k}}}$ are the $\boldsymbol{k}$ vector rotated by $2\pi/3$ and $-2\pi/3$, respectively. The matrix elements in Eqs. (4) and (5) read

$$A(\mathbf{k}) = 2t_{12}\cos(k_y a) + 2t_5 e^{\frac{\sqrt{3}}{2}ik_x a}\cos\left(\tfrac{1}{2}k_y a\right), \tag{6}$$

$$B(\mathbf{k}) = t_2 e^{-i(\frac{1}{2}k_y a - \frac{\sqrt{3}}{2}k_x a)} + t_4 e^{i(\frac{1}{2}k_y a - \frac{\sqrt{3}}{2}k_x a)}, \tag{7}$$

$$\begin{aligned} C(\mathbf{k}) = {} & t_1 e^{-\frac{2\sqrt{3}}{3}ik_x a} + 2t_3 e^{\frac{\sqrt{3}}{6}ik_x a}\cos\left(\tfrac{1}{2}k_y a\right) \\ & + 2t_{14} e^{\frac{\sqrt{3}}{6}ik_x a}\cos\left(\tfrac{3}{2}k_y a\right) + 2t_6 e^{-\frac{5\sqrt{3}}{6}ik_x a}\cos\left(\tfrac{1}{2}k_y a\right) \\ & + 2t_{11} e^{\frac{2\sqrt{3}}{3}ik_x a}\cos(k_y a) + 2t_{13} e^{\frac{\sqrt{3}}{6}ik_x a}\cos\left(\tfrac{3}{2}k_y a\right), \end{aligned} \tag{8}$$

$$\begin{aligned} D(\mathbf{k}) = {} & t_7 e^{-i\frac{\sqrt{3}}{3}k_x a} + t_7 e^{i(\frac{\sqrt{3}}{6}k_x a - \frac{1}{2}k_y a)} + t_8 e^{-i(\frac{\sqrt{3}}{3}k_x a + k_y a)} \\ & + t_9 e^{\frac{2\sqrt{3}}{3}ik_x a} + t_{10} e^{-i(\frac{5\sqrt{3}}{6}k_x a - \frac{1}{2}k_y a)}. \end{aligned} \tag{9}$$

TABLE I. Hopping parameters with relevant hopping distance in the ML-As TB model

i	t_i(eV)	d(Å)	i	t_i(eV)	d(Å)	i	t_i(eV)	d(Å)
1	−3.52	2.51	6	−0.26	5.69	11	0.10	5.69
2	−0.76	3.61	7	0.12	2.51	12	−0.09	3.61
3	0.72	2.51	8	−0.15	4.40	13	−0.07	5.69
4	0.27	3.61	9	−0.10	4.40			
5	0.25	3.61	10	0.10	5.69			

The band structure and density of states (DOS) calculated from the effective Hamiltonian is shown in Fig. 3(a), where the quasiparticle energy within the GW_0 approximation is plotted as a reference. One can see a quite accurate match between the TB model and first-principles calculations. The six bands are almost overlapped with the second and third conduction bands slightly shifted away from the GW_0 bands. Particularly, the VBM is situated right at the Γ point and the CBM is located between the Γ and M point, rendering an indirect energy gap. It is also noted that the band structure matches quite well between −3 and 3 eV, resulting in a good agreement with the DOS.

The accuracy of the TB model for ML-As is quantitatively evaluated by analyzing the energy gap and carrier effective mass (EM), which are highly relevant to the low-energy electronic properties. The energy gaps and EMs at the high-symmetry K points are listed in Table II. Our result shows that the indirect (direct) energy gap obtained from the TB model and quasiparticle energy calculations are 2.79 eV (3.30 eV) and 2.75 eV (3.38 eV), respectively. We also find that both electrons and holes can be well described by the TB model. The EM of electrons at the CBM is 0.41 m_0, close to the value of 0.39 m_0 from the GW_0 calculation. As the first and second valence bands are degenerated at the Γ point, we show the EMs of holes for both bands in the table where one can find that the values are calculated to be 0.44 m_0 and 0.06 m_0, respectively, which are in good agreement with the corresponding GW_0 results of 0.40 m_0 and 0.08 m_0.

Now, we extend our model to the case of an external magnetic field through Peierls substitution in which the hopping term t_{ij} in Eq. (1) is replaced by

$$t_{ij} e^{-i\frac{2\pi}{\Phi_0}e\int_{R_i}^{R_j}\boldsymbol{A}\cdot d\boldsymbol{l}},$$

where $\Phi_0 = hc/e$ and $\boldsymbol{A} = (-By,\ 0,\ 0)$ are the flux quantum and the vector potential in the Landau gauge, respectively. Then, the DOS is calculated for a large sample containing $2\times1000\times2000$ sublattices by means of the tight-binding propagation method [30], where explicit evolution of the current operator is considered instead of diagonalization of large matrices. So far, the highest static magnetic field we

TABLE II. Energy gaps and carrier effective masses of ML-As. The indirect (ΓM) and direct (ΓΓ) energy gaps E_g (in eV) and effective mass for hole and electron (in unit of the free electron mass m_0) at relevant high-symmetry K points of the first Brillouin zone are listed. Γ1 and Γ2 represent the first and second band at the Γ point

	Energy gap (eV)		Holes (m_0)		Electrons (m_0)		
Method	$E_g^{\Gamma M}$	$E_g^{\Gamma\Gamma}$	$m^{\Gamma 1}$	$m^{\Gamma 2}$	m^{Γ}	$m^{\Gamma M}$	m^{K}
DFT-GW	2.75	3.38	0.40	0.08	0.09	0.39	0.37
TB	2.79	3.30	0.44	0.06	0.07	0.41	0.35

know is reported to be 35.5 Tesla (for pulsed magnetic field the value is 58 Tesla) [43], so the magnetic field strength in our simulation is chosen with the same magnitude that is feasible for experimental studies. When the magnetic field $\boldsymbol{B}$ is applied perpendicular to the sheet, the energy levels become quantized, leading to discrete DOS as the Landau Level (LL) peaks. Because the electrons and holes are not symmetric in ML-As, the LLs for them exhibits different distance as shown in Fig. 4. It is also noted that in the low-energy region there are two sets of LLs for holes, and we attribute this to the first and second valence bands, which are degenerated at the Γ point. Generally, these LL spectrum can be simply described by a linear function of the Landau index n within an effective $\boldsymbol{k}\cdot\boldsymbol{p}$ model as

$$\epsilon_{n,s}^{kp} = \epsilon_s + \frac{seB\hbar}{m_0}\left(n + \frac{1}{2}\right)\omega_s, \tag{10}$$

where $s = \pm 1$ denotes the conduction and valence bands, $\epsilon_{+/-} = \epsilon_{c/v}$ is the energy at the conduction and valence edge, and $\omega_s = m_0/m_s^*$ is the relative ratio between free electron and the real system. However, our result shows that the carrier EMs in ML-As are energy-dependent [see Fig. 3(b)], indicating a variable ω_s in Eq. (10), which in return is invalid for the electronic properties investigation with magnetic field. To simplify the problem, we assume that ω_s is a constant and fit the LL spectrum with the data from B = 12.5 T. In this case, we obtain $\epsilon_{+/-} = 1.382$ eV (-1.385 eV) and $\omega_{+/-} = 2.104$ (2.076), respectively, in which the fitted value of the effective mass is comparable to that without magnetic field. The LLs spectrum obtained from our numerical calculations is shown in Fig. 5. Obviously, the LLs spectrum follows a linear dependence on the magnetic field strength and level index in a feasible magnetic field up to 45 T. To check the reliability of our fitted results, we also present the LL energy of B = 25 T as a reference, and one can see that the fitted line coincides with the result from our tight-binding propagation method simulations.

Then, we further investigated the optical properties of ML-As through our TBPM, [8] in which the frequency-dependent optical conductivity (omitting the Drude contribution at $\omega = 0$) is calculated by using the Kubo formula

$$\sigma_{\alpha\beta}(\omega) = \lim_{\epsilon\to 0^+}\frac{e^{-\bar{\beta}\omega}-1}{\omega\Omega}\int_0^\infty e^{-\epsilon t}\sin\omega t \times 2\mathrm{Im}\langle\varphi|f(H)J_\alpha(t)[1-f(H)]J_\beta|\varphi\rangle dt, \tag{11}$$

where $\bar{\beta} = 1/k_BT$ is the inverse temperature, Ω is the sample area, $f(H) = 1/[e^{\bar{\beta}(H-\mu)}+1]$ is the Fermi-Dirac distribution operator, and the time-dependent current operator in the α ($= x$ or y) direction is defined as $J_\alpha(t) = e^{iHt}J_\alpha e^{-iHt}$. Again, we choose the same sample as in the LLs calculation with $\sim 10^6$ atoms and focus on the diagonal components of $\sigma_{\alpha\beta}(\omega)$ only. Our result of the optical conductivity σ_{xx} is shown in Fig. 6 where the magnetic field strength varies from 0 to 50 T. When no external magnetic field is applied ($\mathbf{B} = 0$ T), a sharp increase of σ_{xx} appears around $\omega/t = 3.25$ eV, which corresponds to the direct optical transition from the first VB to the first CB at the Γ point. Thus, our TB model is

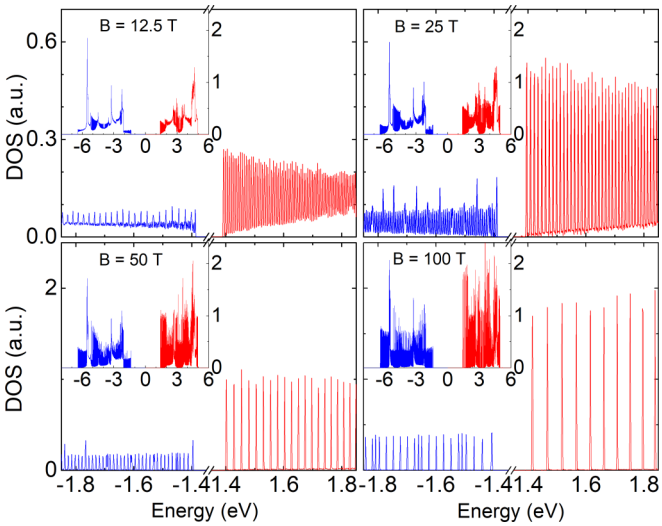

FIG. 4. DOS of ML-As under perpendicular magnetic field. The DOS is extracted from the inset with less dense peaks. Red and blue represents the LLs of electrons and holes, respectively.

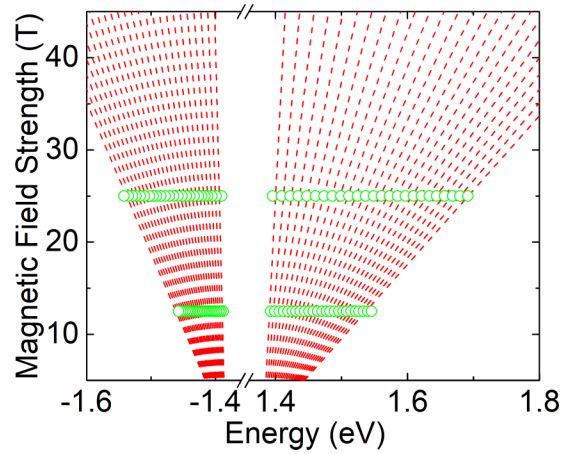

FIG. 5. LL spectrum of ML-As in high magnetic field. The lowest fifty LLs calculated from the linear fitting of Eq. (10) are indicated by the red dashed lines. The green circles are LLs obtained from the tight-binding propagation method.

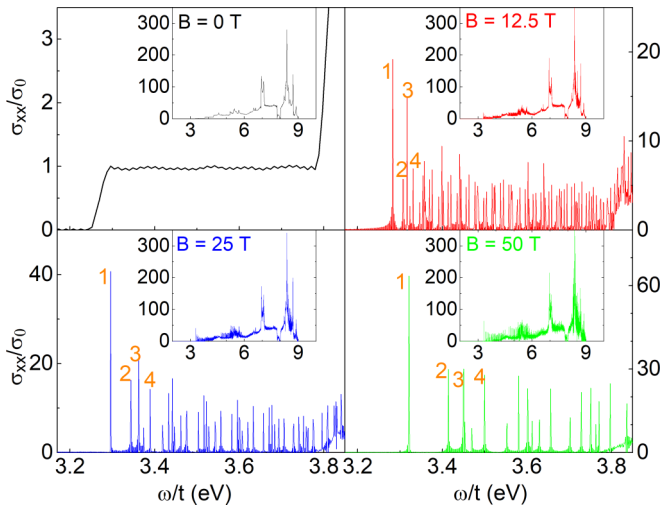

FIG. 6. Magneto-optical properties of ML-As. The optical conductivity spectrum of ML-As is calculated with $\mathbf{B} = 0$ T (black), 12.5 T (red), 25 T (blue), and 50 T (green), respectively. The inset shows the optical conductivity in a much wider energy window. $\sigma_0 = e^2/4\hbar$ is the universal optical conductivity. The first four peaks are present in orange for reference.

further validated by giving a reasonable optical gap comparable to the quasiparticle gap (3.38 eV) obtained from the GW_0 calculation within the random phase approximation. We also noted that the binding energy of the first bound exciton is not neglected. Considering the fact that the main purpose of the optical calculation here is to present the desired spectrum in the framework of the proposed tight-binding model and the treatment of the excitonic effect in the real-space calculations of optical conductivity is much more complicated and requires further exploration, we ignored this effect in the present work.

In the presence of a perpendicular magnetic field, the continuous optical conductivity in the low-energy region becomes quantized with discrete values. To get a clear image of the optical transition, we list the first few peaks of the optical conductivity in Table III. As the strength of the magnetic field increases, the n-th optical conductivity peak shows a blue shift accompanied by a gap broadening. Taking the first four peaks in Fig. 6 as an example, when the magnetic field varies from 12.5 to 50 T, the first and second peak of the optical conductivity increases from 3.282 and 3.307 eV to 3.321 and 3.415 eV, respectively. Our analysis on the optical transition

TABLE III. Optical gap of ML-As under magnetic field. The first four peaks of the optical conductivity calculated from our TB model are listed with $\mathbf{B} = 12.5$, 25, and 50 T, respectively.

	Optical Gap (eV)			
B (T)	1st	2nd	3rd	4th
12.5	3.282	3.307	3.317	3.331
25	3.296	3.344	3.362	3.389
50	3.321	3.415	3.451	3.500

also shows that not all transition is permitted between electrons and holes in ML-As. Taking the first peak with $\mathbf{B} = 50$ T as an example, it originates from the possible transition of carriers in VB_{34}-CB_7 and VB_{15}-CB_{16}, where VB_i and CB_j are the i th and j th LLs of the VB and CB, respectively. To this end, we conclude that the optical conductivity of ML-As with large size can be tuned effectively by the external magnetic field.

IV. CONCLUSION

In summary, we have proposed an effective Hamiltonian for monolayer arsenene that is derived from six p-like orbitals based on the partially self-consistent GW_0 approach. Using this tight-binding model, we can reproduce the electronic and optical properties of ML-As obtained from first-principles calculations, especially, in the low-energy region. By fitting the numerical results from our tight-binding propagation method, we find in ML-As a linear dependence of Landau levels on the perpendicularly applied magnetic field $\mathbf{B}$ and level index n. The optical conductivity spectrum of ML-As also shows a blue shift of the optical conductivity peaks accompanied by a broadening of the gap when the strength of magnetic field increases.

ACKNOWLEDGMENTS

J.Y. acknowledges financial support from MOST 2017YFA0303404, NSAF U1530401 and computational resources from the Beijing Computational Science Research Center. M.I.K. acknowledges financial support from the European Research Council Advanced Grant program (Contract No. 338957). S.Y. acknowledges financial support from the Thousand Young Talent Plan (China).

[1] K. S. Novoselov, D. Jiang, F. Schedin, T. J. Booth, V. V. Khotkevich, S. V. Morozov, and A. K. Geim, Proc. Natl. Acad. Sci. USA **102**, 10451 (2005).
[2] K. F. Mak, C. Lee, J. Hone, J. Shan, and T. F. Heinz, Phys. Rev. Lett. **105**, 136805 (2010).
[3] L. K. Li, Y. J. Yu, G. J. Ye, Q. Q. Ge, X. D. Ou, H. Wu, D. L. Feng, X. H. Chen, and Y. B. Zhang, Nat. Nanotechnol. **9**, 372 (2014).
[4] X. Sun, X. F. Liu, J. Yin, J. Yu, Y. Li, Y. Hang, X. C. Zhou, M. L. Yu, J. D. Li, G. A. Tai, and W. L. Guo, Adv. Funct. Mater. **27**, 1603300 (2017).
[5] M. Naguib, V. N. Mochalin, M. W. Barsoum, and Y. Gogotsi, Adv. Mater. **26**, 992 (2014).
[6] S. L. Zhang, M. Q. Xie, F. Y. Li, Z. Yan, Y. F. Li, E. J. Kan, W. Liu, Z. F. Chen, and H. B. Zeng, Angew Chem. Int. Ed. **55**, 1666 (2016).
[7] M. Pumera and Z. Sofer, Adv. Mater. **29**, 1605299 (2017).
[8] S. J. Yuan, A. N. Rudenko, and M. I. Katsnelson, Phys. Rev. B **91**, 115436 (2015).
[9] A. N. Rudenko, S. Brener, and M. I. Katsnelson, Phys. Rev. Lett. **116**, 246401 (2016).
[10] M. D. Sturge, Phys. Rev. **127**, 768 (1962).

[11] H. M. Manasevit, Appl. Phys. Lett. **12**, 156 (1968).
[12] C. Kamal and M. Ezawa, Phys. Rev. B **91**, 085423 (2015).
[13] Z. Zhu, J. Guan, and D. Tomanek, Phys. Rev. B **91**, 161404 (2015).
[14] Z. Y. Zhang, J. F. Xie, D. Z. Yang, Y. H. Wang, M. S. Si, and D. S. Xue, Appl. Phys. Express **8**, 055201 (2015).
[15] L. Z. Kou, Y. D. Ma, X. Tan, T. Frauenheim, A. J. Du, and S. Smith, J. Phys. Chem. C **119**, 6918 (2015).
[16] J. Zhao, C. Y. Liu, W. L. Guo, and J. Ma, Nanoscale **9**, 7006 (2017).
[17] S. L. Zhang, Z. Yan, Y. F. Li, Z. F. Chen, and H. B. Zeng, Angew. Chem. Int. Ed. **54**, 3112 (2015).
[18] H. Cao, Z. Yu, and P. Lu, Superlattices Microstruct. **86**, 501 (2015).
[19] H. J. Zhang, Y. D. Ma, and Z. F. Chen, Nanoscale **7**, 19152 (2015).
[20] Y. G. Yao, F. Ye, X. L. Qi, S. C. Zhang, and Z. Fang, Phys. Rev. B **75**, 041401 (2007).
[21] C. C. Liu, W. X. Feng, and Y. G. Yao, Phys. Rev. Lett. **107**, 076802 (2011).
[22] A. Acun, L. Zhang, P. Bampoulis, M. Farmanbar, A. van Houselt, A. N. Rudenko, M. Lingenfelder, G. Brocks, B. Poelsema, M. I. Katsnelson, and H. J. W. Zandvliet, J. Phys. :Condens Mattter **27**, 443002 (2015).
[23] S. Mardanya, V. K. Thakur, S. Bhowmick, and A. Agarwal, Phys. Rev. B **94**, 035423 (2016).
[24] J. Zhao, Y. L. Li, and J. Ma, Nanoscale **8**, 9657 (2016).
[25] D. C. Wang, L. Chen, C. M. Shi, X. L. Wang, G. L. Cui, P. H. Zhang, and Y. Q. Chen, Sci. Rep. **6**, 28487 (2016).
[26] Y. P. Wang, W. X. Ji, C. W. Zhang, P. Li, F. Li, M. J. Ren, X. L. Chen, M. Yuan, and P. J. Wang, Sci. Rep. **6**, 20342 (2016).
[27] B. T. Fu, W. X. Feng, X. D. Zhou, and Y. G. Yao, 2D Mater. **4**, 025107 (2017).
[28] Y. Y. Wang, P. Huang, M. Ye, R. Quhe, Y. Y. Pan, H. Zhang, H. X. Zhong, J. J. Shi, and J. Lu, Chem. Mater. **29**, 2191 (2017).
[29] Y. F. Xu, B. Peng, H. Zhang, H. Z. Shao, R. J. Zhang, and H. Y. Zhu, Ann. Phys. (Berlin) **529**, 1600152 (2017).
[30] S. J. Yuan, H. De Raedt, and M. I. Katsnelson, Phys. Rev. B **82**, 115448 (2010).
[31] A. N. Rudenko and M. I. Katsnelson, Phys. Rev. B **89**, 201408 (2014).
[32] A. N. Rudenko, M. I. Katsnelson, and R. Roldán, Phys. Rev. B **95**, 081407 (2017).
[33] D. Kecik, E. Durgun, and S. Ciraci, Phys. Rev. B **94**, 205409 (2016).
[34] N. Marzari and D. Vanderbilt, Phys. Rev. B **56**, 12847 (1997).
[35] N. Marzari, A. A. Mostofi, J. R. Yates, I. Souza, and D. Vanderbilt, Rev. Mod. Phys. **84**, 1419 (2012).
[36] G. Kresse and J. Furthmüller, Phys. Rev. B **54**, 11169 (1996).
[37] G. Kresse and D. Joubert, Phys. Rev. B **59**, 1758 (1999).
[38] J. P. Perdew, K. Burke, and M. Ernzerhof, Phys. Rev. Lett. **77**, 3865 (1996).
[39] P. E. Blöchl, Phys. Rev. B **50**, 17953 (1994).
[40] A. A. Mostofi, J. R. Yates, Y.-S. Lee, I. Souza, D. Vanderbilt, and N. Marzari, Comput. Phys. Commun. **178**, 685 (2008).
[41] S. J. Yuan, T. O. Wehling, A. I. Lichtenstein, and M. I. Katsnelson, Phys. Rev. Lett. **109**, 156601 (2012).
[42] S. J. Yuan, R. Roldan, and M. I. Katsnelson, Phys. Rev. B **84**, 125455 (2011).
[43] Y. Liu, Z. Q. Wang, X. F. Zhang, C. F. Liu, Y. J. Liu, Z. M. Zhou, J. F. Wang, Q. Y. Wang, Y. Z. Liu, C. Y. Xi, M. L. Tian, H. W. Liu, J. Feng, X. C. Xie, and J. Wang, Phys. Rev. X **8**, 021002 (2018).